



**HAL**  
open science

## **Scaling inhibition by sol-gel phosphosilicate hybrid films: Influence of doping Cu<sup>2+</sup> and Zn<sup>2+</sup> cations**

Manel Gritli, H el ene Cheap-Charpentier, Hubert Perrot, Olivier Horner, Yasser  
Ben Amor

### **► To cite this version:**

Manel Gritli, H el ene Cheap-Charpentier, Hubert Perrot, Olivier Horner, Yasser Ben Amor. Scaling inhibition by sol-gel phosphosilicate hybrid films: Influence of doping Cu<sup>2+</sup> and Zn<sup>2+</sup> cations. *Surface and Coatings Technology*, 2022, 443, pp.128597. <10.1016/j.surfcoat.2022.128597>. <hal-03700733>

**HAL Id: hal-03700733**

**<https://hal.science/hal-03700733v1>**

Submitted on 21 Jun 2022

**HAL** is a multi-disciplinary open access archive for the deposit and dissemination of scientific research documents, whether they are published or not. The documents may come from teaching and research institutions in France or abroad, or from public or private research centers.

L'archive ouverte pluridisciplinaire **HAL**, est destin ee au d ep ot et  a la diffusion de documents scientifiques de niveau recherche, publi es ou non,  emanant des  tablissements d'enseignement et de recherche fran ais ou  trangers, des laboratoires publics ou priv es.



HAL Authorization



30 **Abstract**

31 In this work, the scaling protection performance of Zn<sup>2+</sup> and Cu<sup>2+</sup>, added to a phosphosilicate  
32 hybrid sol-gel coating and applied on both carbon and stainless steel surface, was evaluated for  
33 the first time in a solution containing initially 200 mg.L<sup>-1</sup> of Ca<sup>2+</sup> (corresponding to a water  
34 hardness of 50 °F) at 30 °C. Inhibition efficiency was estimated using chronoamperometry (CA)  
35 and quartz crystal microbalance (QCM). Results showed that these smart coatings were  
36 efficient to protect steel surface against scaling phenomenon. The coatings containing the Cu<sup>2+</sup>  
37 inhibitor was the most effective of the systems tested. Moreover, CA and QCM measurements  
38 showed that the formation of calcium carbonate deposition on carbon steel decreased when the  
39 amount of zinc and copper ions added to the sol-gel film increased. Scanning electronic  
40 microscopy and X-ray diffraction results indicated that both cations included in the sol-gel film  
41 affected calcium carbonate nucleation by changing the morphology of CaCO<sub>3</sub> crystals.

42

43

44

45

46

47

48

49 **Keywords:** Scale inhibition, zinc (II) cation, copper (II) cation, sol-gel coating, quartz crystal  
50 microbalance

51

52 **Abbreviations:** EQCM: electrochemical quartz crystal microbalance; CA:  
53 chronoamperometry; QCM: quartz crystal microbalance; SEM: scanning electronic  
54 microscopy; XRD: X-Ray diffraction;

55

## 56 **1. Introduction**

57 The problems related to the scaling phenomena of industrial facilities in contact with waters  
58 become more massive and more insidious. These issues can, as already pointed in numerous  
59 scientific papers, lead to a decrease of the thermal efficiency of the circuit, an obstruction of  
60 pipes as well as the proliferation of living organisms [1-7]. Thus, the economic losses associated  
61 with  $\text{CaCO}_3$  precipitation can be significant [8-10]. To fight this phenomenon, several  
62 protection methods have been applied to preserve installations against scaling. These methods  
63 can be divided into two types: physical and chemical methods. Among the physical methods,  
64 magnetic treatments are generally used [11]. Chemical methods are based on the use of organic  
65 molecules as anti-scalant in numerous situations to prevent scale precipitation [12, 13]. Some  
66 synthetic and natural water-soluble polymers used as scaling inhibitors have been investigated  
67 and reported in literature [12-16]. However, many inhibitors showed up has a secondary effect,  
68 causing damages on the environment. Indeed, poly-phosphonates are very efficient but they can  
69 cause eutrophication when they are rejected in natural waters [17, 18]. Thus, the scientific  
70 community began searching for environmentally friendly inhibitors (green inhibitors) derived  
71 from petrochemicals [14-22], plant extracts [23-33] and chemical modified natural products  
72 from industrial process [34-36]. Nevertheless, the compatibility with the water environment  
73 and the respect of the different safety rules are always questionable even if these products come  
74 from plants or similar. Alternate approach must be found in this context and smart films based  
75 on sol-gel technique can be examined [37]. Materials such as organic-inorganic hybrid  
76 compounds are one of the feasible solutions that enable protection from  $\text{CaCO}_3$  precipitation  
77 reactions during application. They constitute a new generation of multifunctional materials with  
78 useful properties and diverse applications. In addition, polymeric materials are characterized by  
79 their low weight to volume ratio, their excellent resistance to chemical attack, their eco-friendly  
80 properties and their low cost [38]. Further modification of polymer matrix by doping with ions  
81 at low concentrations can proffer superior physical properties of such polymer.

82 The use of eco-friendly sol-gel coatings to prevent scale inhibition can constitute an emerging  
83 area of applications such as it is the case in the corrosion domain [39-45]. In a similar manner,  
84 sol-gel hybrid coatings for metal protection against scaling phenomenon appears as an  
85 interesting field of research. Indeed, it is an attractive technique used to synthesize hybrid  
86 materials with various composition that allow to entrap molecules in an inorganic glassy matrix  
87 [41, 46]. The properties of these sol-gel coatings are strongly dependent on their processing  
88 conditions, pH, temperature and molar ratio of precursors [42, 47]. Silica hybrid sol-gel  
89 coatings are particularly studied and employed for corrosion protection due to their interesting  
90 properties, such as hydrophobicity and good adhesion to metallic substrates [48]. The use of  
91 precursors containing non-hydrolysable bonds allows the organic network to bind directly to  
92 the inorganic network in the structure. Thus, hybrid sol-gel coatings can have the combined  
93 properties of both organic and inorganic functions [43, 44]. The nature of the organic function  
94 (phenyl function, epoxy function, vinyl function and methacrylate function) influences the  
95 properties of the network [39, 49]. The integration of phosphate or phosphonate groups in the  
96 sol-gel network has been published in several works [50-52]. The outcomes proved a good  
97 adhesion to the metallic surface of the film containing phosphorus groups. Santana et al. [49]  
98 studied the effect of the pre-treatment of the carbon steel surface with a phosphoric acid solution  
99 before applying a hybrid sol-gel film. SEM images showed that the pre-treatment step produces  
100 a rougher surface than that of untreated steel. This roughness results in better adhesion of the  
101 sol-gel film to the treated steel substrate. The microstructure of the film obtained by the sol-gel  
102 process depends on the pH of the solution [43, 44]. Therefore, an acid catalysis leads to the  
103 formation of longitudinal fibers and an increase in the condensation generated while a basic  
104 catalysis leads to clusters formation characterized by a spherical shape [53]. Under acidic  
105 conditions, the cation  $H_3O^+$  facilitates the substitution of the OR groups and therefore  
106 hydrolysis. With basic catalysts, the  $OH^-$  anion is attracted towards the electronegative metal  
107 (M) and favours the formation of M-O-M bond by condensation [54, 55]. According to Phan

108 et al. [56], adding phosphoric acid  $H_3PO_4$  provides the most resistant hybrid coating. A denser  
109 network with a greater number of Si–O–P bonds promotes good adhesion to the metallic  
110 surface. The formation mechanism is given in [56] and these authors have used this coating to  
111 study the corrosion of a metallic surface.

112 As it is summarized above, many compounds were applied as scaling inhibitors. All of them  
113 were added to the studied water while the metallic surface treatments such as sol-gel coating  
114 process, were mainly applied to protect metal against corrosion. To our knowledge, no  
115 investigations on the scaling inhibition via sol-gel doped coatings on steel surface in pure  
116 carbonic solution have been performed to date. The present investigation shows the first attempt  
117 to synthesize a sol-gel film on a surface and doped with metallic ions to prevent scale formation.  
118 In this work, hybrid sol-gel coatings were deposited on both carbon steel and stainless steel from  
119 3-[(methacryloyloxy)propyl] trimethoxysilane (MEMO) and bis-[2-(methacryloyloxy) ethyl]  
120 phosphate (BMEP) via sol-gel process (Fig. 1). The experimental procedure is similar to that  
121 adopted by Phan et al. [56]. To improve their anti-scaling properties, deposited coatings were  
122 doped by  $Cu^{2+}$  and  $Zn^{2+}$  cations. Chronoamperometry (CA) and quartz crystal microbalance  
123 (QCM) methods were performed to evaluate the scaling inhibition efficiency of these layers.  
124 To complete the information about the composition and the morphology of the doped sol-gel  
125 coatings, scanning electron microscopy (SEM) observations and X-ray diffraction (XRD)  
126 analysis were done to link the layer properties to the electrochemical and gravimetric  
127 characterizations.

## 128 **2. Materials and methods**

### 129 *2.1. Scaling solution*

130 The synthetic carbonically pure water, containing initially 200 mg.  $L^{-1}$  of  $Ca^{2+}$  (water hardness  
131 of 50 °F), was prepared by dissolving calcium carbonate ( $CaCO_3$ ) powder (VWR AnalaR  
132 NORMAPUR, 99.7% purity) in bi-distilled water. To dissolve calcium carbonate, carbon  
133 dioxide  $CO_2$  gas was introduced in the solution for 24 h with moderate magnetic stirring (450

134 rpm). After the total dissolution of the solid, the pH of the solution was in the range of 5.5 –  
135 5.7. The synthetic water was then filtered using a filter with a porosity of 0.45  $\mu\text{m}$  to remove  
136 impurities.

## 137 2.2. Doping solution

138 Suitable amounts of solutions of analytical grade  $\text{ZnCl}_2$  (Merck, 98 % purity) and  $\text{CuCl}_2 \cdot 2\text{H}_2\text{O}$   
139 (Acros Organics, 99 % purity) were prepared for doping coatings tests. For the doping process,  
140 metallic cations molar quantities ranged from  $10^{-5}$  to  $10^{-3}$  mol.

## 141 2.3. Sol-gel coating solution

142 The sol-gel coating process was applied using 3-[(methacryloyloxy)propyl] trimethoxysilane  
143 (MEMO) and bis [2-(methacryloyloxy) ethyl] phosphate (BMEP) precursors from Sigma-  
144 Aldrich and ethanol provided by VWR. All compounds were used without any further  
145 purification and chemical formulas are given in Fig. 1.

## 146 2.4. Metallic substrate and covered QCM resonators

147 Two different metallic substrates were used in this study. The first one is carbon steel with a  
148 chemical composition (in wt %) of 0.28 % C, 0.28 % Si, 1.25 % Mn, 0.03 % P, 0.16 % Cr, 0.15  
149 % N, 0.07 % Ni, 0.009 % Mo and Fe balance. The carbon steel working electrode, 0.2  $\text{cm}^2$  of  
150 active area, was embedded in inert resin, polished with silicon carbide paper up to 1200 grade  
151 before each experiment. A rotating disk electrode (Tacussel model EDI 101) was used with a  
152 rotation speed ( $\Omega$ ) which was fixed at 500 rpm. The second substrate is based on stainless steel  
153 AISI 316L (Fe/Cr18/Ni10/MO3) sheet (Good fellow, reference FF210320). Thin stainless steel  
154 316L films were prepared on quartz resonators surface using a commercial RF magnetron  
155 sputtering system (Pfeiffer PLS500) from 316L steel disc target of 50 mm diameter. More  
156 precisely, stainless steel was deposited on the gold electrode (0.2  $\text{cm}^2$ ) of the resonators (9 MHz,  
157 AWS Sensors, Spain) to perform QCM-based analysis.

## 158 2.5. Sol-gel coating

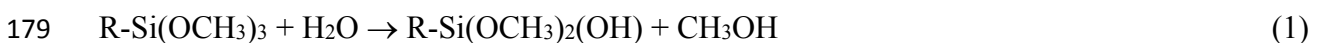
### 159 2.5.1. Pre-treatment of the surface

160 The pre-treatment of the electrode surface was carried out by crystalline phosphating process  
161 with a commercial solution Decorrda 47-15-1 (Klütke). It is a mixture of ethanol (molar  
162 fraction between 50 and 75%) and sodium 3-nitrobenzenesulphonate  $C_6H_4NNaO_5S$  (molar  
163 fraction between 50 and 75% and molecular weight  $225.15 \text{ g}\cdot\text{mol}^{-1}$ ). Crystalline phosphating  
164 process, recommended by Klütke, reduces the flaking surface by forming a phosphate-  
165 converting layer that constitutes a base for bonding the coatings, making the surface rougher  
166 and improving the adhesion of the coating on the metallic surface [56].

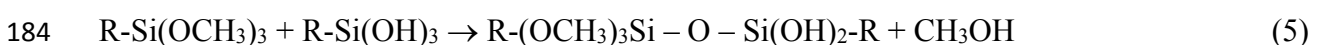
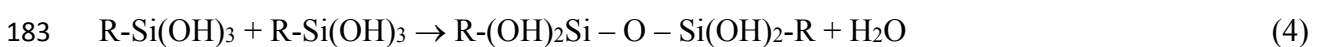
167 The surfaces of 316L steel and carbon steel were pre-treated with a Decorrda 47-15-1  
168 commercial solution for 5 min at a temperature of  $40 \text{ }^\circ\text{C}$ . The increase in temperature is more  
169 favourable to phosphating, which eliminates the presence of iron oxide on the steel surface.

#### 170 2.5.2. Sol-gel preparation

171 The sol-gel process is based on the hydrolysis and condensation reactions of silicon alcoxides  
172  $Si(OR)_n$  in solution (sol) allowing to achieve an infinite viscosity network (gel), where  $n$  is the  
173 oxidation state and OR is an alkoxy group with R an alkyl chain [37]. The most often used  
174 precursors for this type of application are tetra-functional silicon alkoxides of formula  $Si(OR)_4$   
175 [57]. Herein, the sol-gel preparation was done in two stages: hydrolysis (the synthesis of "sol")  
176 following by the condensation (the formation of "gel"). The mechanism was well detailed by  
177 Phan et al. [56]. Hydrolysis of MEMO in aqueous medium took place via  $Si-OCH_3$  methoxy-  
178 silane groups according three successive reactions:



182 Then, condensation reactions occurred according the following reactions:



185

186 The sol-gel procedures used in this work are schematised in Fig. 2. In a first step, MEMO is  
187 hydrolysed in an ethanol/water mixture with MEMO/ethanol/water molar ratio of 1/2/3  
188 (corresponding to the volumes 2.85/1.4/0.65 mL) and then, by stirring at room temperature  
189 during 3h. This selected duration makes it possible to obtain a complete hydrolysis. Ca<sup>2+</sup> and  
190 Zn<sup>2+</sup> cations were injected in the ethanol solution at the beginning with different molar amounts  
191 ranged from 10<sup>-5</sup> mol to 10<sup>-3</sup> mol. Then, 0.3 mL of BMEP was added to the above solution in  
192 order to obtain MEMO/BMEP molar ratio of 10/1 (10Si-1P). This mixture was stirred  
193 vigorously at 65 °C for 1 hour, diluted with 1.61 mL of ethanol to obtain a mass concentration  
194 of 80% of sol-gel in ethanol. Afterwards, the mixture was stirred for at least 15 min until  
195 complete dissolution. The methoxy-silane groups of MEMO precursor are capable to form an  
196 inorganic network Si-O-Si through sol-gel reactions and a polymerizable methacrylate group  
197 capable of producing an organic network. The BMEP precursor containing the functional P-  
198 OH group allows the coating to have good adhesion and a better-condensed inorganic network  
199 by forming strong Fe-O-P bonds with metallic substrates and Si-O-P bonds with a silica  
200 network [56, 58]. The obtained sol-gel films were deposited on polished carbon steel and  
201 stainless steel substrates deposited on the gold electrode of a quartz resonator using a  
202 micropipette (2 µL). The film is maintained at room temperature for 5 min, then, dried at 80 °C  
203 for 20 h, and finally at 120 °C for 2 h in an oven.

## 204 2.6. *Scaling study techniques*

### 205 2.6.1. *Quartz crystal microbalance (QCM)*

206 The piezoelectric properties of the quartz crystal correlate the frequency change and the mass  
207 change deposited on the active surface of quartz crystal according to the Sauerbrey equation [1,  
208 59]:

$$209 \quad \Delta f = -2 \frac{f_0^2}{s\sqrt{\rho\mu}} \Delta m \quad (6)$$

210 where  $\Delta f$  and  $\Delta m$  are the frequency change and the mass change deposited on the electrode  
211 surface, respectively,  $f_0$  is the quartz resonance frequency,  $\rho$ , the quartz density,  $\mu$ , the quartz  
212 shear modulus and  $S$ , the active surface of the quartz given by the shape of one of the gold  
213 electrodes. In a typical QCM set-up, the working electrode is made of a 0.2 cm<sup>2</sup> gold disc  
214 deposited in a 9 MHz AT cut quartz crystal resonator. Typically, the theoretical sensitivity using  
215 Eq. 6 is around 1 ng/Hz. The gold surface of the quartz was previously covered with a layer of  
216 stainless steel 316L covered by a sol-gel film as described in the previous paragraph.  
217 During the QCM test, a volume of 400 ml of the studied synthetic water (carbonically pure  
218 solutions containing 200 mg.L<sup>-1</sup> of Ca<sup>2+</sup>, corresponding to 50 °F) was transferred to a Teflon  
219 container placed in a thermostated bath at 30 °C. CO<sub>2</sub> degassing was achieved by magnetic  
220 stirring at 850 rpm. The degassing of the solution was blocked by stopping the stirring and  
221 closing the opening of the beaker lid in order to block its level of supersaturation corresponding  
222 to a pH of 7.9. Then, a peristaltic pump was used to transfer the solution in the QCM cell. The  
223 QCM setup was monitored by a lab-made software, allowing the recording of the frequency  
224 changes as a function of time. At the end, mass variations over time can be estimated using Eq.  
225 6. Details of this methodology were already given in other works [1, 6].

## 226 2.6.2. Chronoamperometry (CA)

227 CA was used to investigate the scaling process under different conditions [5, 60]. During  
228 measurement, the current was recorded as a function of time at a fixed scaling optimal potential  
229 of -1 V/SCE [60]. Experiments were carried out in a classical three electrodes cell. A saturated  
230 calomel electrode (SCE) was used as a reference electrode. The carbon steel with and without  
231 sol-gel coating acted as a working electrode. The counter electrode was a large platinum grid.

## 232 2.7. Surface characterizations

### 233 2.7.1. SEM observations

234 After each experiment, the morphology of calcium carbonate crystals deposited on both carbon  
235 steel and stainless steel with and without sol-gel coating during the QCM and CA experiments

236 was analysed using scanning electronic microscopy (SEM). The SEM pictures were obtained  
237 on a SEM-FEG Zeiss Ultra55 microscope model. SEM-EDS spectra were recorded using a  
238 Quanta 250 FEG (Field Emission Gun) model accompanied by an EDS detector for elemental  
239 composition measurement, at an accelerating voltage of 10 kV, keeping the magnifications up  
240 to 1,000.000 and 1 nm resolution.

#### 241 2.7.2. X-ray diffraction analysis

242 The XRD spectra were recorded with  $2\theta$  angle in the range of  $20-80^\circ$  with an X-ray  
243 diffractometer type *X-Empyrean Panalytical* employing  $\text{Cu-K}\alpha$  radiation ( $\lambda=1.54 \text{ \AA}$ ).  
244 Intensities of the diffraction peaks at 104 ( $2\theta = 29.5^\circ$ ), 221 ( $2\theta = 46^\circ$ ) and 110 ( $2\theta = 25^\circ$ ) were  
245 used to quantify the calcite, aragonite and vaterite crystallographic forms, respectively. The  
246 calculation of the molar fraction of each variety was reported elsewhere [59].

### 247 3. Results and discussion

#### 248 3.1. Scaling inhibition on sol-gel coating carbon steel electrode

##### 249 3.1.1. Comparison between a bare electrode and a sol-gel coating electrode

250 Firstly, experiments were carried out by chronoamperometry in order to verify if the sol-gel  
251 film could prevent the formation of  $\text{CaCO}_3$  on the electrode. The scaling inhibition of the sol-  
252 gel film was studied on a carbon steel electrode using chronoamperometry and compared to a  
253 bare electrode. Measurements were carried out using a classical rotating disk electrode in a  
254 solution containing initially  $\text{Ca}^{2+}$  ions at a concentration of  $200 \text{ mg.L}^{-1}$  ( $50^\circ\text{F}$ ). A cathodic  
255 potential of  $-1 \text{ V/SCE}$  was applied during the accelerated scaling test to induce the  $\text{CaCO}_3$   
256 electrochemical precipitation [1-3, 6]. The current was normalized by  $I_0$ , which is the current  
257 value at the maximum of the curve. This current-time coordinate system was adopted by  
258 Barchiche et al. [61] to facilitate the comparison between results. The chronoamperometric  
259 curves performed with a bare carbon steel electrode and a carbon steel electrode covered by a  
260 sol-gel film are presented in Fig. 3. The two-recorded curves of Fig. 3 show a similar evolution.  
261 Firstly, an increase of the normalized current is related to the reduction of atmospheric oxides

262 formed on the active area of the working electrode before immersion [5]. Then, a rapid decrease  
263 of  $I/I_0$  was observed and attributed to a fast kinetics of  $\text{CaCO}_3$  deposition on the electrode [3].  
264 The scaling time parameter ( $t_s$ ) can be obtained from chronoamperometric curve (Table 1). As  
265 indicated in Fig. 3, this parameter represents the time needed to lower the current to a stable  
266 value corresponding to the plateau current [62]. For the bare electrode, the  $t_s$  value is 38 min  
267 and the  $I/I_0$  value of the plateau is around 0.19 meaning that the electrode surface was totally  
268 covered by an isolating layer of  $\text{CaCO}_3$ . When the carbon steel electrode was coated by a sol-  
269 gel film, the  $I/I_0$  value of the plateau is obtained more quickly and is higher (0.41) than for a  
270 bare carbon steel electrode. This first result shows that the sol-gel film is porous as the  $\text{O}_2$  can  
271 be reduced on the electrode and acts as a barrier against the formation of  $\text{CaCO}_3$  on the  
272 electrode.

### 273 3.1.2. Scaling on doped sol-gel film coating carbon steel electrode

274 Fig. 4 regroups the chronoamperometric curves recorded during scaling tests on the doped  
275 coating carbon steel electrode polarised at -1 V/SCE for the two doping cations ( $\text{Cu}^{2+}$  and  $\text{Zn}^{2+}$ ).  
276 For the coating doped with  $10^{-5}$  mol of  $\text{Cu}^{2+}$  (blue curve in Fig. 4(a)), the first increase of the  
277 normalized current was not really observed compared to the undoped coating. Then,  $I/I_0$  rapidly  
278 decreased to reach a nearly constant value indicating that the formation of  $\text{CaCO}_3$  on the surface  
279 of the coating was stopped after about 40 min of immersion that correspond to the scaling time.  
280 However, the plateau current was higher than that of undoped coating, which means that  $\text{Cu}^{2+}$   
281 ions prevented slightly the  $\text{CaCO}_3$  formation. For the coating doped with  $10^{-4}$  mol of  $\text{Cu}^{2+}$   
282 (green curve in Fig. 4(a)), the current did not decrease over time so the scaling process was  
283 inhibited during the whole experiment. The scaling time ( $t_s$ ) was undefined. Indeed, practically  
284 no variation of the  $I/I_0$  value was observed during 120 min of experiment which shows that the  
285 kinetics of  $\text{CaCO}_3$  precipitation was extremely slow. For a sol-gel film containing  $10^{-4}$  mol of  
286  $\text{Cu}^{2+}$ , the formation of  $\text{CaCO}_3$  is considered as completely inhibited.

287 Fig. 4(b) shows the chronoamperometric curves for scaling tests on coating doped with  $Zn^{2+}$   
288 cations. Their shapes were similar to that observed for the coating doped with  $10^{-5}$  mol of  $Cu^{2+}$   
289 (blue curve in Fig. 4(a)). The initial decrease of the normalized current was followed by a  
290 plateau of different  $I/I_0$  values depending on the  $Zn^{2+}$  doping cation amount. The scaling time  
291 values were mentioned in Table 1. Higher is the amount of the doping  $Zn^{2+}$ , higher is the scaling  
292 time. Comparing the effect of doping cations, it seems that the inhibitory effect of the film  
293 doped with copper ions is more pronounced than that doped with zinc ions. Indeed, the values  
294 of scaling time mentioned in Table 1 show that  $t_s$  is undefined for  $10^{-4}$  mol of Cu while it is  
295 equal to 51 min for the same amount of  $Zn^{2+}$ .

296 These results obtained by chronoamperometry showed that doping the sol-gel-film with  
297 metallic ions prevented the formation of  $CaCO_3$  on the metallic surface of the electrode. The  
298 sol-gel film with  $Cu^{2+}$  shows a greater inhibition effect than that with  $Zn^{2+}$ .

### 299 *3.2. Sol-gel coating on stainless steel 316L through QCM tool*

300 In order to assess the inhibiting effect of the metallic cations included in the sol-gel film, the  
301 quartz crystal microbalance (QCM) was used to quantify the mass of  $CaCO_3$  nuclei deposited  
302 when the electrode was covered by this coating.

303 The studied solution was prepared by fast controlled precipitation (FCP) in order to bring the  
304 solution to a given sursaturation coefficient [6]. This method allowed forming calcium  
305 carbonate nuclei before precipitation in solution.

#### 306 *3.2.1. Undoped sol-gel film*

307 The mass variations of the  $CaCO_3$  nuclei deposited on stainless steel sol-gel coating electrode  
308 (without and with doping cations) were recorded vs. immersion time in synthetic pure carbonic  
309 solution containing initially  $200 \text{ mg.L}^{-1}$  of  $Ca^{2+}$  (water hardness of  $50 \text{ }^\circ\text{F}$ ) at a sursaturation  
310 coefficient of 32.

311 Firstly, a comparison of the  $CaCO_3$  mass variation deposited was carried out by QCM when the  
312 electrode was covered or not covered by a sol-gel film. The gravimetric curves for a bare

313 stainless steel electrode and for the undoped coating electrode obtained by QCM are presented  
314 in Fig. 5. For the bare stainless steel electrode, the mass of  $\text{CaCO}_3$  increases progressively with  
315 the immersion time without reaching a constant value, even after 120 min of immersion (black  
316 curve in Fig. 5). However, the mass variation ( $\Delta m$ ) of  $\text{CaCO}_3$  deposited on sol-gel coating  
317 stainless steel electrode is different. As it can be observed from the red curve in Fig. 5, an initial  
318 increase of the  $\Delta m$  was clearly recorded for 50 min of immersion. Afterwards,  $\Delta m$  reached a  
319 steady state value about  $42 \mu\text{g}\cdot\text{cm}^{-2}$ . This mass variation means that the active metallic surface  
320 was reduced and the progression of scaling process was stopped. In addition, no loss of mass  
321 has been observed for the sol-gel coating electrode which means that the film is adherent on the  
322 electrode surface. QCM is a suitable technic to control the film adhesion on the electrode  
323 surface. Indeed, if the coating leaves the surface of the QCM or is no longer in contact, there is  
324 a discontinuity in the propagation of the ultrasonic wave that can be detected immediately  
325 thanks to the very high sensitivity of the QCM. Covering stainless steel working electrode with  
326 a phosphosilicate hybrid coating promotes an important reduction of the mass of  $\text{CaCO}_3$   
327 deposit, proving that the sol-gel coating prevents the formation of calcium carbonate on the  
328 metallic surface, even without doping cations.

### 329 *3.2.2. Sol-gel film doped with metallic ions*

330 Fig. 6(a) presents the variation of the mass change of calcium carbonate deposited on sol-gel  
331 coating stainless steel electrode without and with doping  $\text{Cu}^{2+}$  cations. The obtained curves  
332 show an important decrease of the deposit of  $\text{CaCO}_3$  on the doped sol-gel coating with the  
333 increase of cations quantities. Comparing to the undoped system, the steady state was reached  
334 faster leading to a decrease of  $\text{CaCO}_3$  deposit mass. For instance, when the sol-gel film was  
335 doped with  $10^{-5}$  mol of  $\text{Cu}^{2+}$  (red curve in Fig. 6(a)), the mass change reached a steady value  
336 of  $13.8 \mu\text{g}\cdot\text{cm}^{-2}$ . Doping progressively the film with  $\text{Cu}^{2+}$  ions (from  $10^{-5}$  mol and  $10^{-4}$  mol of  
337  $\text{Cu}^{2+}$  added during the preparation of the film) reduces the amount of  $\text{CaCO}_3$  deposited to  $13.8$   
338  $\mu\text{g}\cdot\text{cm}^{-2}$  and  $4.5 \mu\text{g}\cdot\text{cm}^{-2}$ , respectively. The mass change decrease is very important compared

339 to the quantity of  $\text{CaCO}_3$  deposited on the undoped coating ( $42 \mu\text{g}\cdot\text{cm}^{-2}$ ) which reflects the  
340 particularly pronounced effect of copper ions on the improvement of the anti-scale effectiveness  
341 of sol-gel films. Scaling parameters, such as nucleation time ( $T_N$ ), scaling gravimetric time ( $T_S$ )  
342 and scaling rate ( $V_S$ ) were extrapolated from the gravimetric curves as defined by Tlili et al.  
343 [63]. The corresponding values are given in Table 2. The increase of  $\text{Cu}^{2+}$  doping cation amount  
344 influences mainly the scaling rate ( $V_S$ ) that was reduced from  $2.21 \mu\text{g cm}^{-2} \text{min}^{-1}$  (undoped film)  
345 to  $0.15 \mu\text{g cm}^{-2} \text{min}^{-1}$  for the film doped with  $10^{-4}$  mol of  $\text{Cu}^{2+}$ . The values of  $T_N$  and  $T_S$  for  
346 doped system are higher than that of the undoped system.

347 The effect of  $\text{Zn}^{2+}$  doping cations on the anti-scaling properties of the sol-gel phosphosilicate  
348 hybrid coating was also studied by QCM. Four amounts of  $\text{Zn}^{2+}$  cations ranged from  $10^{-5}$  mol  
349 to  $10^{-2}$  mol were also examined. The extrapolated scaling parameters are also added to the Table  
350 2 and the corresponding recorded gravimetric curves are shown in Fig. 6(b). The increasing  
351 amounts of  $\text{Zn}^{2+}$  cations in the sol-gel film progressively inhibit the formation of scale on the  
352 surface of the sol-gel phosphosilicate hybrid coating. The mass of calcium carbonate decreases  
353 from  $42 \mu\text{g}\cdot\text{cm}^{-2}$  to  $7 \mu\text{g}\cdot\text{cm}^{-2}$ . The  $V_S$  value (Table 2) decreases from  $1.46 \mu\text{g}^{-1} \text{cm}^{-2} \text{min}^{-1}$  to  
354  $0.39 \mu\text{g}\cdot\text{cm}^{-2}\cdot\text{min}^{-1}$  when  $\text{Zn}^{2+}$  molar quantity increases from  $10^{-5}$  mol to  $10^{-3}$  mol. The value  
355 of  $T_N$  seems to be independent of the doping process while the values of  $T_S$  for doped system  
356 are higher than those characteristic of scaling on undoped coating (Table 2).

357  $\text{Zn}^{2+}$  doping cations, as well as  $\text{Cu}^{2+}$ , improved the anti-scaling effect of the studied sol-gel film.  
358 However, these results confirmed that  $\text{Cu}^{2+}$  ions are more efficient than  $\text{Zn}^{2+}$  ions towards scale  
359 deposition. Indeed, for a sol-gel film doped with  $\text{Cu}^{2+}$  and  $\text{Zn}^{2+}$  at  $10^{-4}$  mol, the amount of  
360  $\text{CaCO}_3$  deposits was  $4.5 \mu\text{g}\cdot\text{cm}^{-2}$  and  $13 \mu\text{g}\cdot\text{cm}^{-2}$  respectively (Fig. 6). This difference  
361 corroborates the result obtained by chronoamperometry for carbon steel, confirming the anti-  
362 scaling properties of the studied sol-gel coating.

363 The inhibition effect of cations was assumed to be due to the weak release of the ions in the  
364 solution. Indeed, some experiments were carried out by spectrophotometry UV-Vis (data not

365 shown here) in order to detect the presence of cations in the solution. The results showed that a  
366 very small quantity of cations was released from the sol-gel film towards the solution. As a  
367 consequence, the scaling inhibition is mainly related to an interfacial effect.

### 368 3.2.3. SEM micrographs and XRD analysis on 316L stainless steel

369 SEM images of the sol-gel film and CaCO<sub>3</sub> formed on the surface of 316L stainless steel, under  
370 different experimental conditions (undoped and doped with ions), are shown in Fig. 7 and Fig.  
371 8 for Cu<sup>2+</sup> and Zn<sup>2+</sup> respectively. The molar fractions of vaterite, aragonite and calcite  
372 calculated from XRD spectra are presented in Table 3.

373 Fig. 7a shows the presence of small CaCO<sub>3</sub> crystals formed on the sol-gel coating without  
374 doping cations covering the surface of the stainless steel 316L electrode. The shapes of the  
375 crystals are difficult to identify. However, the presence of calcite has been confirmed by XRD  
376 analysis as shown in Fig. 7(d), which revealed characteristic peaks of this crystalline variety.  
377 When the sol-gel coating was doped with 10<sup>-5</sup> and 10<sup>-4</sup> mol of Cu<sup>2+</sup> (Figs. 7(b) and (c)  
378 respectively), SEM images show that the deposit was mainly formed by circular crystal typical  
379 of vaterite [5, 6], which is confirmed by XRD analysis (Fig. 7(e) and (f)). In addition, the  
380 presence of Cu<sup>2+</sup> ions decreased the number of CaCO<sub>3</sub> crystals deposited on the doped sol-gel  
381 film. On the film doped with Cu<sup>2+</sup>, XRD analysis (Fig. 7(e)) confirmed the presence of both  
382 calcite and vaterite as observed in the SEM images of Fig. 7(b).

383 The morphology of CaCO<sub>3</sub> scale formed on the surface of the hybrid coating doped with Zn<sup>2+</sup>  
384 are shown in Fig. 8. When the sol-gel film is doped with 10<sup>-5</sup> mol of Zn<sup>2+</sup>, vaterite form is  
385 observed (Fig. 8(a)) which is confirmed by the XRD spectrum in Fig. 8(e). Calcite appear when  
386 the doping cations rises to 10<sup>-4</sup> to 10<sup>-3</sup> mol, as it can be observed in the Fig. 8(b) and (c) and  
387 Table 3. Doping the sol-gel coating with 10<sup>-2</sup> mol of Zn<sup>2+</sup> lead to the aragonite formation (Fig.  
388 8(d) and Table 3). The presence of these CaCO<sub>3</sub> crystallographic forms was also confirmed by  
389 X-ray diffraction analysis (Fig. 8 (e) to (h)). XRD spectra were also recorded on coating doped  
390 with different amounts of Zn<sup>2+</sup> cation. Results are in agreement with SEM observations (Fig.

391 8(a) to (d)). For  $10^{-5}$  mol to  $10^{-3}$  mol of doping  $Zn^{2+}$  cation, vaterite and calcite were the  
392 constituents of the  $CaCO_3$  deposit (Fig. 8(e) to (g) and Table 3). With  $10^{-2}$  mol of doping  $Zn^{2+}$ ,  
393 X-ray analysis (Fig. 8(h) and Table 3) showed the presence of aragonite.

394 The molar fractions of observed crystalline varieties formed on sol gel coating stainless steel  
395 electrode (Table 3) were estimated using the calculation method described in a previous paper  
396 [59]. The calculated values shown in Table 3 are dependent on the doping cations amount  
397 indicating the inhibiting role of this added ions on the scaling process and the  $CaCO_3$  structure.

398 The molar fractions of vaterite and calcite decreased when the molar quantities of ions  
399 increased. It can be noted the appearance of aragonite for a sol-gel film doped with  $10^{-2}$  mol of  
400  $Zn^{2+}$  at a molar fraction of 24% (Table 3). The inhibition effect of  $Cu^{2+}$  and  $Zn^{2+}$  cations added  
401 to the coating hybrid structure was demonstrated as it was the case when they were injected in  
402 solution as soluble scaling inhibitor [59, 64-66]. Gritli et al. [59] have demonstrated by FCP a  
403 total efficiency of  $Cu^{2+}$  and  $Zn^{2+}$  in solution for a concentration of 5 and 4  $mg.L^{-1}$  respectively.  
404 Other authors [65] have determined with the same technique lower concentrations for the  
405 inhibition of  $CaCO_3$  formation (0.5  $mg.L^{-1}$  of  $Cu^{2+}$  and 0.15  $mg.L^{-1}$  of  $Zn^{2+}$ ). Zeppenfeld [66]  
406 have showed an inhibition efficiency at about 90% for a concentration superior at 2  $mg.L^{-1}$  of  
407  $Cu^{2+}$ . To conclude this part, the doped sol-gel film acts as an antiscaling barrier.

#### 408 **4. Conclusion**

409 The present study was devoted to investigate the anti-scaling performance of a sol-gel  
410 phosphosilicate hybrid coating doped with copper or zinc cations deposited onto two different  
411 metals, largely used in the water domain, stainless 316L steel and carbon steel. The outcomes  
412 allow the following conclusions to be drawn:

- 413 1. An hybrid doped sol-gel phosphosilicate coating was successfully applied onto stainless  
414 and carbon steel surfaces. The anti-scaling proprieties of this film was demonstrated  
415 under different experimental conditions.

- 416 2. The different techniques of investigations (QCM and CA) confirmed that doping the  
417 hybrid coating with  $\text{Cu}^{2+}$  and  $\text{Zn}^{2+}$  cations delayed the scaling process proving the  
418 scaling inhibiting performance of this doped film in synthetic water containing initially  
419  $200 \text{ mg.L}^{-1}$  of  $\text{Ca}^{2+}$  (water hardness of  $50 \text{ }^\circ\text{F}$ ).
- 420 3. Crystalline form of  $\text{CaCO}_3$  appeared at the studied interface. They were mainly  
421 influenced by the amount of  $\text{Zn}^{2+}$  and  $\text{Cu}^{2+}$  doping cations that are included in the  
422 different films.
- 423 4. Surface analysis techniques (SEM and X-ray diffraction) supported investigations and  
424 confirmed the anti-scaling properties of the doped coatings.

425

426

427

428

#### 429 **Acknowledgements**

430 This work was supported by PHC-Utique program 18G1218 (MES-DGRS Tunisia), 39229 TA  
431 (Campus France), Erasmus Plus program and the Islamic Development Bank (BID). The  
432 authors thank Françoise Pillier, Cyrille Bazin and Axel Desnoyers de Marbaix (LISE) for  
433 technical assistance.

434

435

436 **References**

- 437 [1] Y. Chao, O. Horner, F. Hui, J. Lédion, H. Perrot, Direct detection of calcium carbonate  
438 scaling via a pre-calcified sensitive area of a quartz crystal microbalance. *Desalination* 352  
439 (2014) 103-108.
- 440 [2] D. Peronno, H. Cheap-Charpentier, O. Horner, H. Perrot, Study of the inhibition effect of  
441 two polymers on calcium carbonate formation by fast controlled precipitation method and  
442 quartz crystal microbalance. *J. Water Process Eng.* 7 (2015) 11-20.
- 443 [3] Y. Ben Amor, L. Bousselmi, B. Tribollet, E. Triki, Study of the effect of magnesium  
444 concentration on the deposit of allotropic forms of calcium carbonate and related carbon steel  
445 interface behavior. *Electrochim. Acta* 55 (2010) 4820-4826.
- 446 [4] Y. Ben Amor, L. Bousselmi, E. Sutter, J.P. Labbé, E. Triki, C. Fiaud, Apport de la  
447 microbalance à quartz dans l'étude de l'influence des ions sulfate, chlorure et magnésium sur la  
448 cinétique d'entartrage. *Mater. Tech.* 92 (2004) 53-61.
- 449 [5] Y. Ben Amor, L. Bousselmi, M.C. Bernard, B. Tribollet, Nucleation-growth process of  
450 calcium carbonate electrodeposition in artificial water-Influence of the sulfate ions. *J. Cryst.*  
451 *Growth* 320 (2011) 69-71.
- 452 [6] H. Cheap-Charpentier, O. Horner, J. Lédion, H. Perrot, Study of the influence of the  
453 supersaturation coefficient on scaling rate using the pre-calcified surface of a quartz crystal  
454 microbalance. *Water Res.* 142 (2018) 347-353.
- 455 [7] N. Chhim, E. Haddad, T. Neveux, C. Bouteleux, S. Teychené, B. Biscans, Performance of  
456 green antiscalants and their mixtures in controlled calcium carbonate precipitation conditions  
457 reproducing industrial cooling circuits. *Water Res.* 186 (2020) 116334.
- 458 [8] J. MacAdam, S.A. Parsons, Calcium carbonate scale control, effect of material and  
459 inhibitors. *Water Sci. Technol.* 49 (2004) 153–159.

- 460 [9] K. Touati, E. Alia, H. Zendah, H. Elfil, A. Hannachi, Sand filters scaling by calcium  
461 carbonate precipitation during groundwater reverse osmosis desalination. *Desalination* 430  
462 (2018) 24-32.
- 463 [10] A. Korchef, M. Touaibi, Effect of pH and temperature on calcium carbonate precipitation  
464 by CO<sub>2</sub> removal from iron-rich water. *Water Environ. J.* 34 (2020) 331-341.
- 465 [11] A. Al Helal, A. Soames, S. Iglauer, R. Gubner, A. Barifcani, The influence of magnetic  
466 fields on calcium carbonate scale formation within monoethylene glycol solutions at  
467 regeneration conditions. *J. Pet. Sci. Eng.* 173 (2019) 158–169.
- 468 [12] M. Chaussemier, E. Pourmohtasham, D. Gelus, N. Pécou, H. Perrot, J. Lédion, H. Cheap-  
469 Charpentier, O. Horner, State of art of natural inhibitors of calcium carbonate scaling. A review  
470 article. *Desalination* 356 (2015) 47–55.
- 471 [13] H. Zahlan, S.W. Saeed, R. Alrasheed, N.M. Alandes, T. Aouak, Synthesis of poly (citric  
472 acid-co-glycerol) and its application as an inhibitor of CaCO<sub>3</sub> deposition. *Materials* 12 (2019)  
473 3800.
- 474 [14] S.R. Popuri, C. Hall, C.C. Wang, C.Y. Chang, Development of green/biodegradable  
475 polymers for water scaling applications. *Int. Biodeterior. Biodegrad.* 95 (2014) 225-231.
- 476 [15] L. Guangqing, M. Xue, H. Yang, Polyether copolymer as an environmentally friendly scale  
477 and corrosion inhibitor in seawater. *Desalination* 419 (2017) 133–140.
- 478 [16] Z. Xu, Y. Zhao, J. Wang, H. Chang, Inhibition of calcium carbonate fouling on heat  
479 transfer surface using sodium carboxymethyl cellulose. *Appl. Therm. Eng.* 148 (2019) 1074–  
480 1080.
- 481 [17] J.A. Camargo, A. Alonso, Ecological and toxicological effects of inorganic nitrogen  
482 pollution in aquatic ecosystems: A global assessment. *Environ. Int.* 32 (2006) 831-849.
- 483 [1] N. Belkin, E. Rahav, H. Elifantz, N. Kress, I. Berman-Frank, The effect of coagulants and  
484 antiscalants discharged with seawater desalination brines on coastal microbial communities: A

485 laboratory and in situ study from the southeastern Mediterranean. *Water Res.* 110 (2017) 321-  
486 331.

487 [18] N. Belkin, E. Rahav, H. Elifantz, N. Kress, I. Berman-Frank, The effect of coagulants and  
488 antiscalants discharged with seawater desalination brines on coastal microbial communities: A  
489 laboratory and in situ study from the southeastern Mediterranean. *Water Res.* 110 (2017) 321-  
490 331.

491 [19] S. M. Thombre, B.D. Sarwade, Synthesis and biodegradability of polyaspartic acid: a  
492 critical review. *J. Macromol. Sci.* 42 (2005) 1299–1315.

493 [20] M. Euvrad, A. Martinod, A. Neville, Effects of carboxylic polyelectrolytes on the growth  
494 of calcium carbonate. *J. Cryst. Growth* 317 (2011) 70–78.

495 [21] Z. Quan, Y. Chen, X. Wang, C. Shi, Y. Liu, C.F. Ma, Experimental study on scale  
496 inhibition performance of a green scale inhibitor polyaspartic acid. *Sci. China B Chem.* 51  
497 (2008) 695–699.

498 [22] J. Chen, L. Xu, J. Han, M. Su, Q. Wu, Synthesis of modified polyaspartic acid and  
499 evaluation of its scale inhibition and dispersion capacity. *Desalination* 358 (2015) 42–48.

500 [23] A.M. Abdel-Gaber, B.A. Abd-El-Nabey, E. Khamis, D.E. Abd-El-Khaled, Investigation  
501 of fig leaf extract as a novel environmentally friendly antiscalant for CaCO<sub>3</sub> calcareous  
502 deposits. *Desalination* 230 (2008) 314–328.

503 [24] A.M. Abdel-Gaber, B.A. Abd-El-Nabey, E. Khamis, D.E. Abd-El-Khaled, A natural  
504 extracts scale and corrosion inhibitor for steel surface in brine solution, *Desalination* 278 (2011)  
505 337–342.

506 [25] A.M. Abdel-Gaber, B.A. Abd-El-Nabey, E. Khamis, H. Abd-El-Rhmann, H. Aglan, A.  
507 Ludwick, Green anti-scalant for cooling water systems. *Int. J. Electrochem. Sci.* 7 (2012)  
508 11930–11940.

509 [26] M. Bonoli, A. Bendini, L. Cerretani, G. Lercker, T.G. Tosci, Qualitative and semi  
510 quantitative analysis of phenolic compounds in extra virgin olive oils as a function of the

511 ripening degree of olive fruits by different analytical techniques. *J. Agric. Food Chem.* 52  
512 (2004) 7026–7032.

513 [27] G. Maciejewska, W. Zierkiewicz, A. Adach, M. Kopacz, I. Zapala, I. Bulik, M. Cies'lak-  
514 Golonka, T. Grabowski, J. Wietrzyk, A typical calcium coordination number: physicochemical  
515 study, cytotoxicity, DFT calculations and in silico pharmacokinetic characteristics of calcium  
516 caffates. *J. Inorg. Biochem.* 103 (2009) 1189–1195.

517 [28] O.H. Lee, B.Y. Lee, J. Lee, H.B. Lee, J.Y. Son, C.S. Park, K. Shetty, Y.C. Kim,  
518 Assessment of phenolics-enriched extract and fractions of olive leaves and their antioxidant  
519 activities. *Bioresour. Technol.* 100 (2009) 6107–6113.

520 [29] C. Woodward, E.A. Davidson, Structure-function relationships of protein polysaccharide  
521 complexes: specific ion-binding properties. *Proc. Natl. Acad. Sci. U. S. A.* 60 (1986) 201–205.

522 [30] Z. Belarbi, J. Gamby, L. Makhloufi, B. Scotta, B. Tribollet, Inhibition of calcium carbonate  
523 precipitation by aqueous extracts of *Paronychia argentea*. *J. Cryst. Growth* 386 (2014) 208–  
524 214.

525 [31] T. Lourteau, H. Berriche, K. Kécili, V. Heim, D. Bricault, M. Litaudon, X. Cachet, F.  
526 Roussi, H. Perrot, O. Horner, H. Cheap-Charpentier, Scale inhibition effect of *Hylocereus*  
527 *undatus* solution on calcium carbonate formation. *J. Cryst. Growth* 524 (2019) 125-161.

528 [32] O. Horner, H. Cheap-Charpentier, X. Cachet, H. Perrot, J. Lédion, D. Gelus, N. Pécoul,  
529 M. Litaudon, F. Roussi, Antiscalant properties of *Herniaria glabra* aqueous solution.  
530 *Desalination* 409 (2017) 157–162.

531 [33] H. Cheap-Charpentier, D. Gelus, N. Pécoul, H. Perrot, J. Lédion, O. Horner, J. Sadoun, X.  
532 Cachet, M. Litaudon, F. Roussi, Antiscalant properties of *Spergularia rubra* and *Parietaria*  
533 *officinalis* aqueous solutions. *J. Cryst. Growth* 443 (2016) 43–49.

534 [34] X. Qiang, Z. Sheng, H. Zhang, Study on scale inhibition performances and interaction  
535 mechanisms of modified collagen. *Desalination* 309 (2013) 237-242.

536 [35] H. Zhang, F. Weng, X. Jin, H. Zhu, A botanical polysaccharide extracted from abandoned  
537 corn stalks: modification and evaluation of its scale inhibition and dispersion performance.  
538 *Desalination* 326 (2013) 55-61.

539 [36] W. Yu, Y. Wang, A. Li, H. Yang, Evaluation of the structural morphology of starch-graft-  
540 poly (acrylic acid) on its scale-inhibition efficiency. *Water Res.* 141 (2018) 86-95.

541 [37] D. Wang, G.P. Bierwagen, Sol-gel coatings on metals for corrosion protection. *Prog. Org.*  
542 *Coat.* 64 (2009) 327-338.

543 [38] P. Rodič, M. Lekka, F. Andreatta, L. Fedrizzi, I. Milošev, The effect of copolymerisation  
544 on the performance of acrylate-based hybrid sol-gel coating for corrosion protection of  
545 AA2024-T3. *Prog. Org. Coat.* 147 (2020) 105701.

546 [39] S. Zheng, J. Li, Inorganic-organic sol-gel hybrid coatings for corrosion protection of  
547 metals. *J. Sol-Gel Sci. Technol.* 54 (2010) 174-187.

548 [40] M. Catauro, F. Bollino, F. Papale, R. Giovannardi, P. Veronesi, Corrosion behavior and  
549 mechanical properties of bioactive sol-gel coatings on titanium implants. *Mater. Sci. Eng. C.*  
550 43 (2014) 375-382.

551 [41] E. Roussi, A. Tsetsekou, A. Skarmoutsou, C.A. Charitidis, A. Karantonis, Anticorrosion  
552 and nanomechanical performance of hybrid organo-silicate coatings integrating corrosion  
553 inhibitors. *Surf. Coat. Technol.* 232 (2013) 131-141.

554 [42] R.B. Figueira, C.J.R. Silva, V. Pereira, Hybrid sol-gel coating for corrosion protection of  
555 hot-dip galvanized steel in alkaline medium. *Surf. Coat. Technol.* 265 (2015) 191-204.

556 [43] M. Mrad, Y. Ben Amor, L. Dhouibi, M.F. Montemor, Corrosion prevention of AA2024-  
557 T3 alloy with a polyaniline/poly ( $\gamma$ -glycidoxypropyltrimethoxysilane) bi-layer coating:  
558 Comparative study with polyaniline monolayer feature. *Surf. Coat. Technol.* 337 (2018) 1-11.

559 [44] M. Mrad, Y. Ben Amor, L. Dhouibi, F. Montemor, Effect of AA2024-T3 surface pre-  
560 treatment on the physicochemical properties and the corrosion performance of poly ( $\gamma$ -  
561 glycidoxypropyltrimethoxysilane) sol-gel coating. *Surf. Interface Anal.* (2017) 1-11.

562 [45] R. del Olmo, U. Tiringier, I. Milošev, P. Visser, R. Arrabal, E. Matykina, J.M.C. Mol,  
563 Hybrid sol-gel coatings applied on anodized AA2024-T3 for active corrosion protection. Surf.  
564 Coat. Technol. 419 (2021) 127251.

565 [46] A. Suárez-Vega, C. Agustín-Sáenz, L.A. O'Dell, F. Brusciotti, A. Somers, M. Forsyth,  
566 Properties of hybrid sol-gel coatings with the incorporation of lanthanum 4-hydroxy cinnamate  
567 as corrosion inhibitor on carbon steel with different surface finishes. Appl. Surf. Sci. 561 (2021)  
568 149881.

569 [47] R.B. Figueira, Hybrid sol-gel coatings for corrosion mitigation: A critical review,  
570 Polymers 12 (2020) 689.

571 [48] R.V. Lakshmi, S. Sampath, S.T. Aruna, Silica-alumina based sol-gel coating containing  
572 cerium oxide nanofibers as a potent alternative to conversion coating for AA2024 alloy. Surf.  
573 Coat. Technol. 411 (2021) 127007.

574 [49] I. Santana, A. Pepe, E. Jimenez-Pique, S. Pellice, S. Ceré, Silica-based hybrid coatings for  
575 corrosion protection of carbon steel. Part I: Effect of pretreatment with phosphoric acid. Surf.  
576 Coat. Technol. 236 (2013) 476–484.

577 [50] A.N. Khramov, V.N. Balbyshev, L.S. Kasten, R.A. Mantz, Sol-gel coating with  
578 phosphonate functionalities for surface modification of magnesium alloys. Thin Solid Films  
579 514 (2006) 174–181.

580 [51] A.G. Kannan, N.R. Choudhury, N.K. Dutta, Synthesis and characterization of methacrylate  
581 phosphor-silicate hybrid for thin film applications. Polymers 48 (2007) 7078–7086.

582 [52] A.G. Kannan, N.R. Choudhury, N.K. Dutta, Electrochemical performance of sol-gel  
583 derived photo-silicate-methacrylate hybrid coating. J. Electroanal. Chem. 641 (2010) 28– 34.

584 [53] Y. Xiao, J. Shen, Z. Xie, B. Zhou, G. Wu, Microstructure control of nanoporous silica thin  
585 film prepared by sol-gel process. J. Mater. Sci. Technol. 23 (2007) 504–508.

586 [54] C.L. Chiang, C.C.M. Ma, D.L. Wu, H.C. Kuan, Preparation, characterization and  
587 properties of novolac-type phenolic/SiO<sub>2</sub> hybrid organic-inorganic nanocomposite materials by  
588 sol-gel method. *J. Polym. Sci., Part A: Polym. Chem.* 41 (2003) 905–913.

589 [55] J.-P. Bonino, E. Xuereb, J. Esteban, F. Ansart, Les revêtements sol-gel pour  
590 l'anticorrosion. *Mater. Tech.* 99 (2011) 41–50.

591 [56] T.T. Phan, F. Bentiss, C. Jama, Effects of sol-gel process parameters on the anticorrosive  
592 performance of phosphosilicate hybrid coatings for carbon steel: structural and  
593 electrochemical studies. *New J. Chem.* 42 (2018) 13442-13452.

594 [57] J. Livage, Les procédés sol-gel, de l'art feu à la chimie douce, *l'Act. Chim.* 10 (1997) 4-  
595 10.

596 [58] S. Kirtay, Preparation of hybrid silica sol-gel coatings on mild steel surfaces and  
597 evaluation of their corrosion resistance. *Prog. Org. Coat.* 77 (2014) 1861–1866.

598 [59] M. Gritli, H. Cheap-Charpentier, O. Horner, H. Perrot, Y. Ben Amor, Scale inhibition  
599 properties of Cu<sup>2+</sup> and Zn<sup>2+</sup> cations in hard water by using a pre-calcified quartz crystal  
600 microbalance. *Desalin. Water Treat.* 167 (2019) 113-121.

601 [60] J. Lédion, P. Leroy, J.P. Labbe, Détermination du caractère incrustant d'une eau par un  
602 essai d'entartrage accéléré, *TSM- L'eau* 80 (1985) 323–328.

603 [61] C. Barchiche, C. Deslouis, O. Gil, S. Joiret, P. Refait, B. Tribollet, Role of sulphate ions  
604 on the formation of calcareous deposits on steel in artificial seawater; the formation of Green  
605 Rust compounds during cathodic protection, *Electrochim. Acta* 54 (2009) 3580 –3588.

606 [62] C. Garcia, G. Courbin, F. Ropital, C. Fiaud, Study of the scale inhibition by HEDP in a  
607 channel flow cell using a quartz crystal microbalance, *Electrochim. Acta* 46 (2001) 973–985.

608 [63] M.M. Tlili, M. Ben Amor, C. Gabrielli, S. Joiret, G. Maurin, P. Rousseau, Study of  
609 Electrochemical Deposition of CaCO<sub>3</sub> by *In Situ* Raman Spectroscopy. *J. Electrochem. Soc.*  
610 150, (2003) C485-C493.

- 611 [64] A. Gutjahr, H. Dabringhaus, R. Lacmann, Studies of the growth and dissolution kinetics  
612 of the CaCO<sub>3</sub> polymorphs calcite and aragonite, II. The influence of divalent cation additives  
613 on the growth and dissolution rates. *J. Cryst. Growth* 158 (1996) 310-315.
- 614 [65] H.S. Ras, S. Ghizellaoui, Influence of copper and zinc on the power furring of encrusting  
615 water. *Energy Procedia*. 18 (2012) 1511-1522.
- 616 [66] K. Zeppenfeld, Prevention of CaCO<sub>3</sub> scale formation by trace amounts of copper (II) in  
617 comparison to zinc (II). *Desalination* 252 (2010) 60-65.
- 618
- 619